

# A new paradigm for the X-ray emission of O stars from *XMM-Newton* observations of the O9.7 supergiant $\zeta$ Orionis $\star$

A. M. T. Pollock

European Space Agency *XMM-Newton* Science Operations Centre, European Space  
Astronomy Centre, Apartado 50727, Villafranca del Castillo, 28080 Madrid, Spain.

Received 2005 July 15 / Accepted 2006 November 09

**Abstract.** *XMM-Newton* observations of the O supergiant  $\zeta$  Orionis (O9.7 Ib) extend knowledge of its high-resolution spectrum beyond the C VI line at  $33.7\text{\AA}$  and suggest a new framework for the interpretation of the X-ray spectra of single hot stars. All the lines are broad and asymmetric with similar velocity profiles. X-rays probably originate in the wind's terminal velocity regime in collisionless shocks controlled by magnetic fields rather than in cooling shocks in the acceleration zone. During post-shock relaxation, exchange of energy between ions and electrons is so slow that electron heating does not take place before hot gas is quenched by the majority cool gas. The observed plasma is not in equilibrium and the electron bremsstrahlung continuum is weak. Charge exchange, ionization and excitation are likely to be produced by protons. Fully thermalized post-shock velocities ensure high cross-sections and account for the observed line widths, with some allowance probably necessary for non-thermal particle acceleration. In general, the form of X-ray spectra in both single and binary stars is likely to be determined principally by the amount of post-shock electron heating: magnetically confined X-ray plasma in binary systems can evolve further towards the higher electron temperatures of equilibrium while in single stars this does not take place. The long mean-free path for Coulomb energy exchange between fast-moving ions may also inhibit the development of line-driven instabilities.

**Key words.** X-rays : stars – Stars : early-type – Stars : individual :  $\zeta$  Orionis – Stars : winds, outflows – Shock waves

## 1. Introduction

The O9.7 Ib supergiant  $\zeta$  Orionis, or Alnitak, is the easternmost star of Orion's belt and lies just above the Horsehead Nebula. In addition to its glorious appearance in the night sky, it is a prominent star in other respects. It is optically the brightest O star and, at X-ray frequencies, it is the seventh most luminous in absolute terms and the fourth in apparent brightness (Berghöfer et al., 1996). Waldron & Cassinelli (2001) observed it early with the *Chandra* high-energy gratings to yield one of the first published high-resolution X-ray spectra and argued for the origin of at least some of the X-rays very close to the stellar surface at the base of the powerful wind that is a ubiquitous feature of such hot stars. The intensity ratios of the He-like triplets, which are susceptible to modification by the strong photospheric UV radiation field, were used to locate the site of production.

Its X-ray spectrum has proved to be typical of those seen from O stars with very prominent broad lines from a variety of H-like and He-like ions of common light elements and L-shell lines from Fe xvii in particular. Miller et al. (2002) and Miller (2002) commented on the unexpected and little understood line widths observed from star to star and made general efforts to reconcile the data with the popular view that shocks developing from instabilities in the wind line-driving mechanism are responsible for generating the X-rays. Whatever their origin, Feldmeier et al. (1997) suggested that X-ray temperature shocks cool very rapidly via radiation losses in the inner wind, probably accounting for the range of temperatures of one to a few million degrees observed in even comparatively low-resolution ROSAT PSPC spectra. It is clear from the high-resolution spectra that a range of apparent temperatures is implied by the simultaneous presence of prominent lines such as O vii typical of 0.8MK gas; O viii of 2.4MK; Fe xvii of 4MK; and Si xiii of 10MK.

*XMM-Newton* is ideal for observations of such hot stars. The bandwidth of the Reflection Grating Spectrometer (RGS) matches perfectly that part of the X-ray spectrum in which the lines occur, extending the *Chandra* High-Energy Transmission Grating (HETG) spectra beyond 25Å to the N vi lines near 29Å and C vi near 34Å into the temperature regime below a million degrees where the radiative emissivity increases rapidly. The RGS is able to resolve the lines and its high sensitivity allows the accumulation of enough statistics to study line profiles in detail.

The supergiant in which we are interested is the dominant component of a multiple system (Hummel et al., 2000) and is more properly known as  $\zeta$  Orionis Aa, though we refer to it simply as  $\zeta$  Orionis throughout. Its fainter companions are  $\zeta$  Orionis Ab at 0.045'' and  $\zeta$  Orionis B at 2.4'', neither of which is likely to contribute to the X-ray emission; and  $\zeta$  Orionis C at 58'', which would be easily resolvable by all the *XMM* instruments.  $\zeta$  Orionis B was resolved in the *Chandra* observation at an intensity of a few percent of  $\zeta$  Orionis. Some relevant parameters which we have adopted for  $\zeta$  Orionis are listed in Table 1. Because the terminal velocity is an important

---

\* Based on observations obtained with *XMM-Newton*, an ESA science mission with instruments and contributions directly funded by ESA Member States and NASA

parameter, it is worth bearing in mind that earlier work by Prinja et al. (1990) preferred a value of  $1860 \text{ km s}^{-1}$ , the difference probably reflecting the uncertainty in such measurements.

**Table 1.** Relevant data for HD37742 O9.7Ib  $\zeta$  Orionis from Lamers et al. (1999) unless stated otherwise.

visual magnitude	$V$	2.03	
effective temperature	$T_{\text{eff}}$	30900 K	
radius	$R_*$	$31 R_{\odot}$	
terminal velocity	$v_{\infty}$	$2100 \text{ km s}^{-1}$	
mass-loss rate	$\dot{M}$	$1.4 \times 10^{-6} M_{\odot} \text{ yr}^{-1}$	
distance	$d$	473 pc	de Zeeuw et al. (1999)
interstellar column density	$N_{\text{H}}$	$2.5 \times 10^{20} \text{ cm}^{-2}$	Diplas & Savage (1994)

## 2. Observations

The European Space Agency’s *XMM-Newton* Observatory (Jansen et al., 2001) has been in operation since 1999. Some of its operational and instrumental characteristics and a range of initial astrophysical results were described in the special 2001-01-01 issue of *Astronomy & Astrophysics*, including the high-resolution RGS spectrometers by den Herder et al. (2001) and the EPIC imaging moderate-resolution spectrometers by Strüder et al. (2001) and Turner et al. (2001). *XMM* was used to observe  $\zeta$  Orionis for nearly 12 hours in September 2002 as part of guaranteed time. All the instruments operate simultaneously except, in this case, the Optical Monitor (OM) (Mason et al., 2001), which was not used because of the extreme optical brightness of the target. Some observational details are shown in Table 2. The data were reduced with standard procedures using the *XMM* Science Analysis System SASv6.5.0 with the calibration data available up to July 2005.

The combined RGS spectrum in Fig. 1 shows that the type of strong lines seen in the HETG spectra below  $25 \text{ \AA}$  continue to the longest RGS wavelengths. The He-like O VII triplet was the strongest line followed by O VIII Ly $\alpha$ ; the Fe XVII lines between 15 and 17  $\text{\AA}$ ; and the strong detection of C VI Ly $\alpha$  near 34  $\text{\AA}$ . Where they overlap between about 6 and 25  $\text{\AA}$ , the RGS and HETG spectra are essentially identical as discussed in more detail below.

The EPIC spectra are shown in slightly different form in Fig. 2 without any effective area corrections as this becomes misleading when the energy resolution is relatively poor. Nonetheless, the EPIC data complement the RGS because of their higher sensitivities, as emphasized by the detected count rates in Table 2, and wider bandwidths. Both pn and MOS show that almost all  $\zeta$  Orionis’s X-rays fall in the RGS waveband. At short wavelengths beyond the strong MOS detections of the He-like triplets Mg XI and Si XIII, apart from weak detections of Si XIV and S XV, there is no evidence of a hard X-ray tail. At the longest wavelengths, the counts are over-

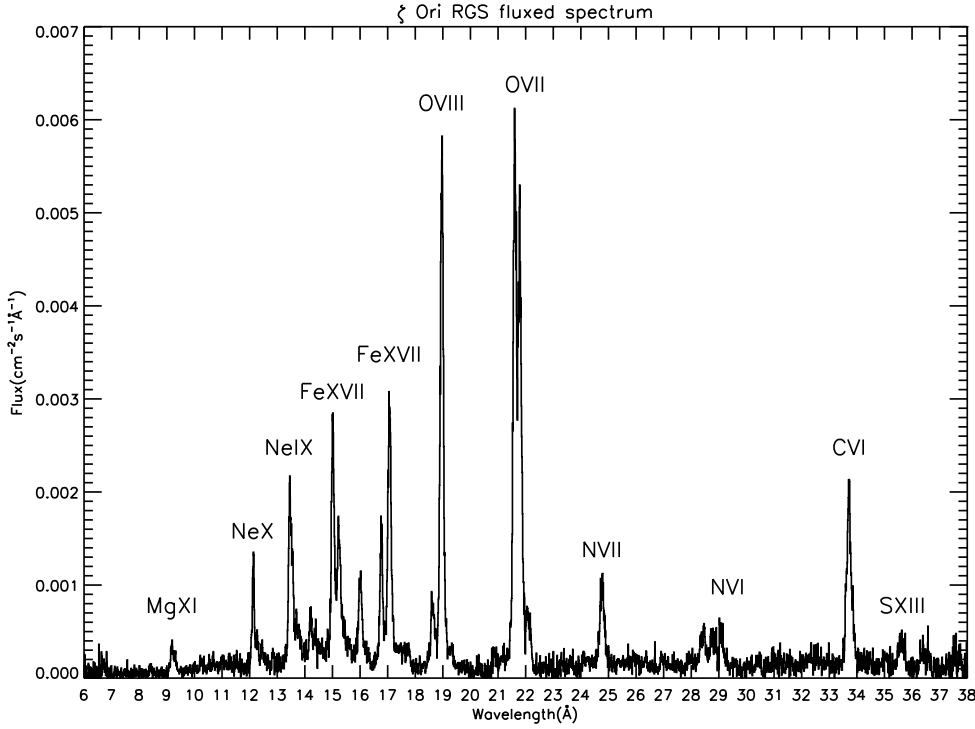


**Fig. 1.** The RGS spectrum of  $\zeta$  Orionis on 2002-09-15. The spectrum is a combination of all the available RGS1 and RGS2 1st and 2nd order data corrected for instrumental sensitive area using the SAS task `rgsfluxer`.

whelmingly due to redistribution from higher energies as the CCD energy resolutions deteriorate due to surface effects. Despite the limited ability to distinguish individual lines, the high pn count rate provides the most effective means of assessing source variability of which there was none detectable during this observation. Berghöfer & Schmitt (1994) made a variability study of  $\zeta$  Orionis with *ROSAT* and found effectively no evidence for either short-term or long-term variability although there was one isolated episode during which the X-ray count rate increased by 15%.

**Table 2.** *XMM-Newton*  $\zeta$  Orionis observation log showing the background-corrected count rates. The RGS values are the 1st order rates.

Instrument	Filter	Mode	Start and End Dates		Duration(s)	Count Rate(s <sup>-1</sup> )
RGS1	...	Spec+Q	2002-09-15T13:11:17	2002-09-16T00:52:38	41979	0.346±0.003
RGS2	...	Spec+Q	2002-09-15T13:11:17	2002-09-16T00:52:38	41979	0.322±0.003
MOS1	Thick	Small Window	2002-09-15T13:12:32	2002-09-16T00:51:00	41728	1.735±0.007
MOS2	Thick	Timing	2002-09-15T13:12:28	2002-09-16T00:46:41	41473	1.692±0.006
pn	Thick	Full Frame	2002-09-15T14:04:08	2002-09-16T00:51:20	38362	6.659±0.014

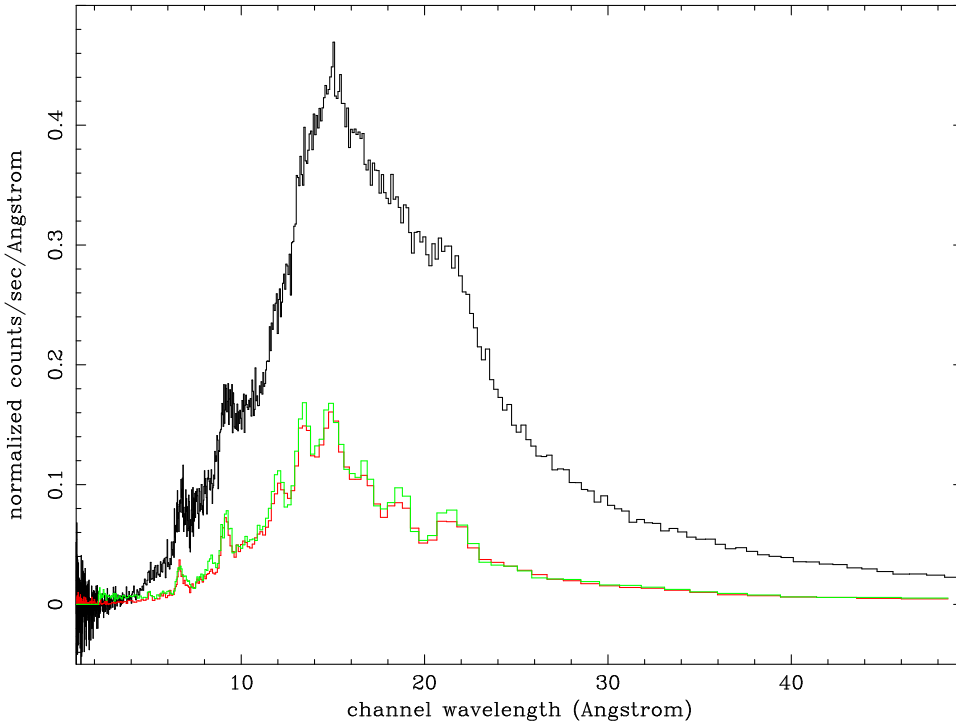


**Fig. 2.** Spectra of  $\zeta$  Orionis on 2002-09-15 from the three EPIC instruments. The pn, shown in black, had the highest count rate mainly because it does not share its telescope module with an RGS. The MOS instruments have better energy resolution and were able to separate lines reasonably well. The agreement was good between MOS1 and MOS2 which were operated in different modes. MOS1, shown in red, was in small-window imaging mode while MOS2 was in timing mode.

### 3. Shape and strength of X-ray lines in $\zeta$ Orionis

Comparison, for example, of the Ly $\alpha$  lines of C vi  $\lambda$ 33.734 and Ne x  $\lambda$ 12.132 separated by nearly a factor of 3 in wavelength shows they had shapes in velocity space that were very similar as shown in Fig. 3. This similarity appears to apply to all the lines and we have been able to synthesize a good fit to the entire observed high-resolution spectrum with the same velocity profile for every line. In order to model the type of line asymmetries in  $\zeta$  Puppis discovered by Kahn et al. (2001) and Cassinelli et al. (2001), we added to XSPEC<sup>1</sup> a local triangular line-profile model named TriLine characterized, as illustrated in Fig. 4, by three shape parameters: independent red and blue velocities where the profile goes to zero and a velocity shift of the central peak from the laboratory wavelength.

The model included 85 lines from 18 ions with TriLine profiles, with laboratory wavelengths taken from the APED (Smith et al., 2001) and CHIANTI (Young et al., 2003) line lists, and a thermal continuum subject to interstellar absorption fixed at the value given in Table 1. The 18 model ions were the H-like ions of C vi, N vii, O viii, Ne x, Mg xii and Si xiv; the He-like

<sup>1</sup> <http://xspec.gsfc.nasa.gov/docs/xanadu/xspec/index.html>

ions of N VI, O VII, Ne IX, Mg XI and Si XIII; Fe XVII-XXI; and S XII-XIII. The Lyman series lines were explicitly treated as doublets with the flux ratio fixed at 2:1. The continuum was intended to account empirically for the combination of true electron continuum and other lines. The nature of the continuum is discussed further below in Section 4.

Fits were not made to fluxed spectra like that plotted in Fig. 1 but to the detected counts spectra using the appropriate response matrices. Many spectral bins contain few or even zero counts. For such photon-limited data to which Poissonian rather than Gaussian statistics apply, a likelihood measure like that provided by XSPEC's C-statistic is the correct choice rather than a  $\chi^2$ -statistic. Errors reported in this paper were calculated for  $\Delta C = 1$ .

The best-fit parameters reported in Tables 3 and 4 were calculated for a combined fit to the spectra of RGS1 and RGS2 1st and 2nd order and the *Chandra* MEG and HEG  $\pm 1$  spectra retrieved from the public archive.

These models were a significant technical challenge with the large number of different lines and spectra involved, to accommodate which an expanded version of XSPEC v11 was built. There were 3472 parameters in the model which reduced to 84 for the single line profile once all the constraints were applied through XSPEC's Tcl script capabilities.

The RGS and HETG spectra, which were taken over two years apart, agree well with each other both in the shapes of the lines and in overall luminosity to within 10 or 20% as shown in Table 4. The single line-profile fits showed very similar red and blue velocities with a significant asymmetry due to a blue-shift of the line peak. The velocity errors are small by virtue of combining several hundred independent estimates of a single profile from the lines of different spectra. The statistical errors take no account of any systematic differences between lines although the model-independent and statistical analyses reported below and the comparisons between data and model shown in Fig. 5 all suggest that the common profile gives a good representation. It establishes that the peak of the X-ray lines in  $\zeta$  Orionis is significantly blue-shifted by about  $-300\text{km s}^{-1}$ , similar though not as much as the shift in  $\zeta$  Puppis. The values of blueV and redV are 80% of  $\zeta$  Orionis's terminal velocity of  $v_\infty = 2100\text{km s}^{-1}$  or 90% of the preferred value of Prinja et al. (1990). They are accurate enough to compare with any of the velocity parameters used to describe the complex shape of UV P Cygni profiles that trace cool pre-shock material.

In order to help comparison with earlier work and allow an assessment of the significance of the line asymmetry, we also implemented a SkewLine model of a Gaussian line with different blue and red velocity half widths. Table 5 shows the results of a number of TriLine and SkewLine fits subject to different shift and symmetry constraints. The fits are of the same data and can thus be compared quantitatively with the likelihood C-statistic. The best of the eight fits in the Table is the blue-shifted SkewLine model which gives very similar parameters for the mean velocity distribution of line-emitting material as the best TriLine model. It is clear, in particular from comparison with the best-fit symmetrical unshifted models, that the mean line is very significantly skewed and blue-shifted. The symmetrical Gaussian results agree well with those reported earlier by Miller (2002) for the *Chandra* data.

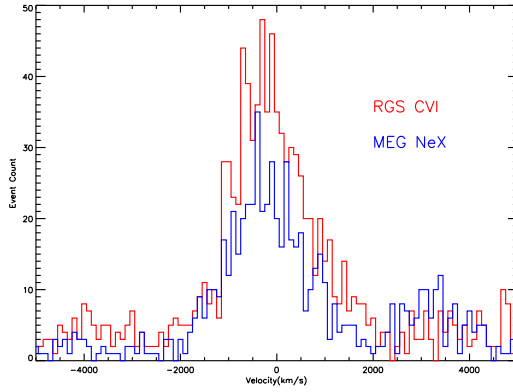


**Fig. 3.** The RGS C VI and MEG Ne x Ly $\alpha$  velocity profiles of  $\zeta$  Orionis. The resolutions of the two instruments are roughly the same in velocity units at these wavelengths, allowing direct comparison of the two profiles. The MEG feature at about  $+3000 \text{ km s}^{-1}$  is due to Fe xvii and Fe xxi .

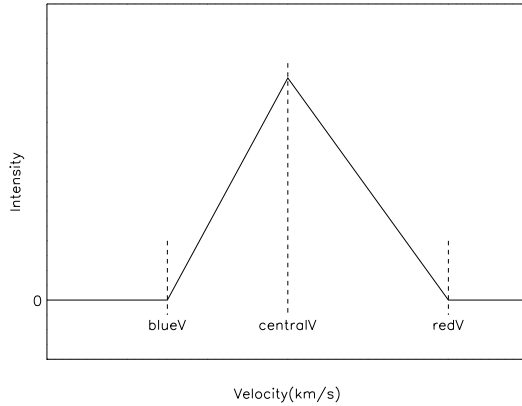


**Fig. 4.** The TriLine model incorporated into XSPEC to describe the X-ray lines of  $\zeta$  Orionis. A similar SkewLine model with unequal red and blue Gaussian widths was also used.

Although the asymmetrical SkewLine gives a better fit, we prefer the more convenient TriLine parameterisation that is easier to relate to other observable quantities, velocity measurements and the line models calculated in the literature. The superiority of the SkewLine model may be related to ability of its wings to help account for weaker neighbouring lines not included in the model line list. In any case, longer-exposure data would allow a more reliable statistical comparison. With the single shifted, asymmetric TriLine model of Table 3 for  $\zeta$  Orionis, the line fluxes listed in Table 7 were determined, where no corrections for absorption were made. Here too, the measurements in common agree well with Miller's.

**Table 3.**  $\zeta$  Orionis best-fit emission-line velocity parameters and underlying continuum for the simultaneous multiple common-profile **TriLine** **XSPEC** model fit to the *XMM-Newton* RGS 1st and 2nd order spectra of 2002-09-15 and *Chandra* MEG and HEG  $\pm 1$  order spectra of 2000-04-08.

TriLine velocities		
blueV	$-1642 \pm 22$	$\text{km s}^{-1}$
centralV	$-302 \pm 29$	$\text{km s}^{-1}$
redV	$+1646 \pm 26$	$\text{km s}^{-1}$
bremsstrahlung continuum		
$N_{\text{H}}$	$2.5 \times 10^{20}$	$\text{cm}^{-2}$
kT	$0.494 \pm 0.007$	keV
normalisation	$5.66 \pm 0.14 \times 10^{-3}$	
C-statistic=22862.4 using 26281 PHA bins		

**Table 4.** Best-fit normalisation parameters for the model of Table 3. **TriLine** model fit to high-resolution spectra of  $\zeta$  Orionis taken with *XMM-Newton* on 2002-09-15 and *Chandra* on 2000-04-08.

Instrument	Order	Counts	Relative Normalisation
RGS1	-1	15136	$1.02 \pm 0.01$
RGS2	-1	14133	1
RGS1	-2	2771	$1.13 \pm 0.01$
RGS2	-2	2507	$1.00 \pm 0.01$
MEG	-1	5556	$1.11 \pm 0.02$
MEG	+1	3568	$1.03 \pm 0.02$
HEG	-1	1129	$1.18 \pm 0.03$
HEG	+1	839	$1.12 \pm 0.03$



**Table 5.** Best-fit emission-line velocity parameters in  $\text{km s}^{-1}$  for variously constrained **TriLine** and blue and red half-Gaussian **SkewLine** model fits to the grating spectra of  $\zeta$  Orionis from the *XMM-Newton* RGS and the *Chandra* MEG and HEG.

	blueV	centralV	redV	C-stat	constraint
TriLine	$-1642 \pm 22$	$-302 \pm 29$	$+1646 \pm 26$	22864.4	Best fit of Table 3
TriLine	$-1641 \pm 15$	$-303 \pm 26$	$+1641 \pm 15$	22865.9	$ \text{redV}  =  \text{blueV} $
TriLine	$-1774 \pm 21$	0	$+1492 \pm 21$	22973.1	centralV=0
TriLine	$-1684 \pm 15$	0	$+1684 \pm 15$	23053.2	centralV=0, $ \text{redV}  =  \text{blueV} $
	blueW	centralV	redW	C-stat	constraint
SkewLine	$650 \pm 25$	$-318 \pm 29$	$991 \pm 27$	22816.7	
SkewLine	$811 \pm 9$	$-126 \pm 10$	$811 \pm 9$	22879.4	redW=blueW
SkewLine	$880 \pm 12$	0	$738 \pm 12$	22947.6	centralV=0
SkewLine	$841 \pm 10$	0	$841 \pm 10$	23038.4	centralV=0, redW=blueW

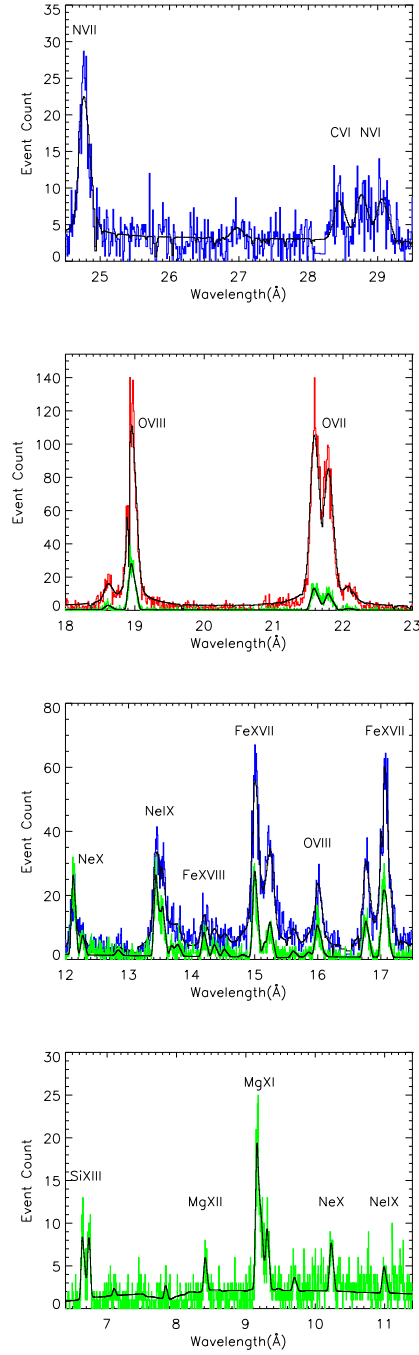


**Fig. 5.** Selected comparisons of high-resolution X-ray data with the best-fit single mean *TriLine* profile model used for all the lines with the 1st order RGS1 in red, RGS2 in blue and the combined MEG 1st order in green. The common model is shown by the smooth black line. The O VIII  $\text{Ly}\alpha$  line was affected by bad pixels in RGS1.

### 3.1. The composite model-independent line profile

The important model-independent question arises of whether any X-ray gas was observed at velocities greater than  $v_\infty$ . We have calculated the distribution of all the detected events in velocity space by stacking all the individual line velocity distributions. Any continuum or background photons should form a smooth background in the composite velocity space. The resultant profiles from both *XMM* and *Chandra* data are shown in Fig. 6. It should be emphasized that this plot has limitations in that it includes the instrumental resolutions and neglects sensitivity variations, such as bad pixels, that are properly taken into account in the response matrices; the RGS 1st order profile, for example, was affected by CCD columns missing near the centre of the O VIII Ly $\alpha$   $\lambda$ 18.967. As these defects have nothing to do with the distribution of moving gas in  $\zeta$  Orionis, we should be able assess reasonably objectively from the ensemble of lines the range of velocities present. Taking into account the differing resolving power in the four spectra, they agree well with each other and with the TriLine velocities reported in Table 3. The blue wing is sharp and joins the weak underlying continuum before the terminal velocity is reached. The red wing, on the other hand, flattens above about +1000 km s<sup>-1</sup> because of the strength of the He-like triplet intercombination lines. It is quite safe to conclude from Fig. 6 that there was no X-ray emitting gas moving at or above the wind terminal velocity.

### 3.2. An assessment of line-profile variations

The sharpness of the composite line profile is consistent with the idea suggested by Fig. 3 that all ions have much the same shape. In order to check this more rigorously, we have estimated individual best-fit line profiles for the most prominent ions as reported in Table 6. As well as showing the individual ion TriLine parameters, the statistical significance of the differences may be judged using  $\Delta C$ , the decrease in the value of the C-statistic gained by freeing an ion's TriLine parameters. Under the null hypothesis of a common line profile,  $\Delta C$  should be distributed as  $\chi^2_3$  for the 3 extra degrees of freedom. The variations between ions are small, amounting to less than about 200 km s<sup>-1</sup> from one ion to another, but probably real. Nevertheless, the assumption of a single profile looks like a sensible working hypothesis.

It has been argued by both Kahn et al. (2001) and Cassinelli et al. (2001) that the N VII Ly $\alpha$  line in  $\zeta$  Puppis has a much wider flat-topped profile, significantly different from the other lines, so that a single shape does not apply. However, the RGS data of  $\zeta$  Puppis suggest that the N VII line might not be unusually wide if account is taken of blending with N VI He $\beta$ : the N VI He-like triplet is strong and in common with N VII Ly $\beta$  and C VI Ly $\alpha$  is not obviously unusually broad. We intend to discuss  $\zeta$  Puppis in detail in a future article. In  $\zeta$  Orionis, the evidence from Table 6 and Fig.7 is that the longest-wavelength C VI line is, if anything, narrower than average rather than broader.

**Table 6.** Best-fit TriLine model velocity parameters for individual prominent ions in the X-ray spectrum of  $\zeta$  Orionis compared with the single common line model. The quoted  $1\sigma$  errors were estimated using the XSPEC> `error 1.` command

ion	blueV (km s <sup>-1</sup> )	centralV (km s <sup>-1</sup> )	redV (km s <sup>-1</sup> )	C-stat	$\Delta C$
All ions	-1642±22	-302±29	+1646±26	22862.4	
C VI	-1719±135	-270±137	+1403±130	22855.6	6.8
N VII	-1705±55	-111±240	+1065±324	22859.8	2.6
O VII	-1349±72	-509±83	+1835±76	22844.9	17.5
O VIII	-1656±43	-258±59	+1482±46	22838.7	23.7
Fe XVII	-1647±42	-421±62	+1845±59	22848.9	13.5
Ne IX	-1653±77	-211±79	+1508±102	22859.9	2.5
Ne X	-1730±106	-327±126	+1735±103	22861.0	1.4
Mg XI	-1536±153	+33±121	+1487±144	22850.1	12.3
Mg XII	-721±365	-662±227	+1514±471	22855.1	7.3
Si XIII	-1449±124	+48±240	+1421±188	22856.4	6.0

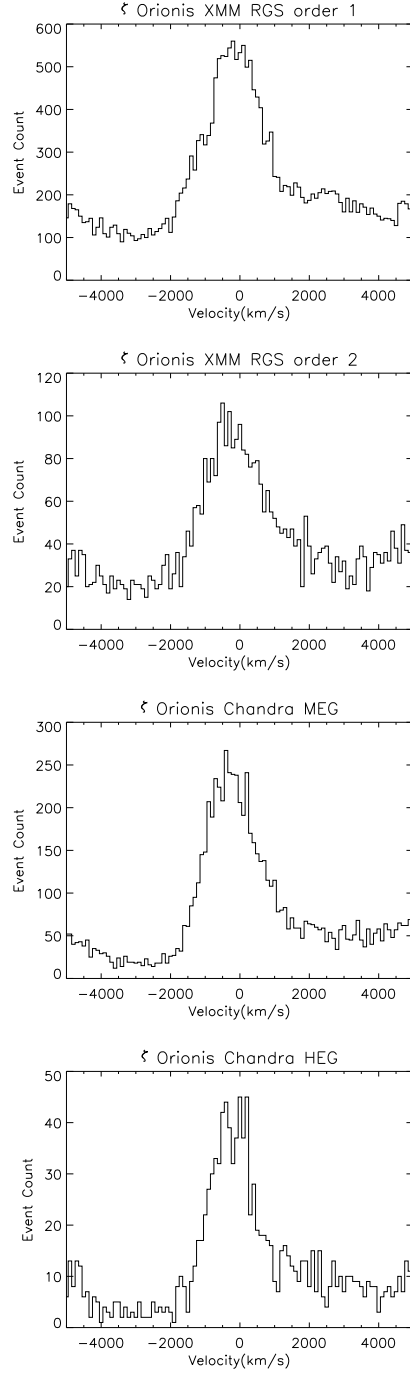


**Fig. 6.** Composite X-ray line profiles of  $\zeta$  Orionis calculated from *XMM-Newton* RGS and *Chandra* HETG grating data. The instrumental resolution improves down the page so that the observed profile becomes a better approximation to the actual velocity dispersion of X-ray emitting material. The profile at  $v > +1000 \text{ km s}^{-1}$  is distorted by the intercombination lines of the He-like triplets.  $\zeta$  Orionis's terminal velocity is  $v_{\infty} = 2100 \text{ km s}^{-1}$ .

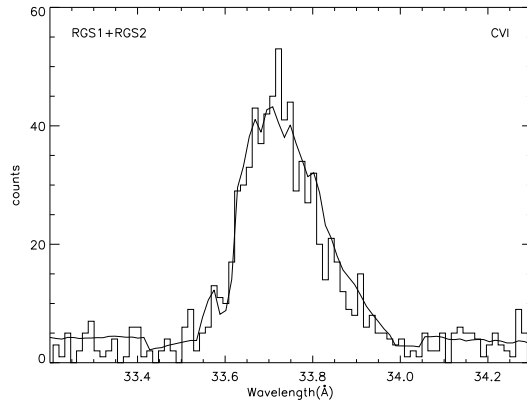


**Fig. 7.** The C VI Ly $\alpha$  line of  $\zeta$  Orionis observed with the *XMM-Newton* RGS shown by the histogram compared with the mean TriLine model profile of the joint fit of Table 3 to all the lines in the spectrum.

#### 4. The X-ray continuum in $\zeta$ Orionis

Although a semi-empirical continuum component was added to the line models described above, the real nature and strength of the continuum is an important matter as it is a direct diagnostic of the density and temperature of plasma electrons. In common with other O-stars, the continuum is weak. Not only are lines responsible for the most obvious features in the spectrum in Fig. 1, but increasing numbers of weaker lines seem to make up most of the emission observed. Fig. 8 shows details of the spectrum between 17 and 19 Å. The low flux between about 17.8 and 18.5 Å, that contrasts to the plateau immediately bluewards, is common to the handful of O stars observed so far but still shows features that could plausibly be identified with upper level transitions of Fe xviii for which no observed wavelengths are available in the line lists. The flux reached similarly low but again not especially smooth values between 20 and 21 Å, where plausible identifications are with lines of N vii and Ca xvii.

The high-resolution X-ray spectra of well known relatively high-temperature active cool stars, such as AB Dor and HR 1099, show obvious strong continuum emission, although this is not the case with cooler stars such as Procyon (Raassen et al., 2002), where the continuum is notably weak. We considered global empirical line+continuum models for  $\zeta$  Orionis with more than the 85 lines already included but these soon became impractical as the number of weak lines increases exponentially and the wavelengths are uncertain. If a continuum is present in  $\zeta$  Orionis, its flux near 18Å is less than about  $5 \times 10^{-5} \text{cm}^{-2} \text{s}^{-1} \text{Å}^{-1}$ . A long exposure would help to constrain it with more confidence.

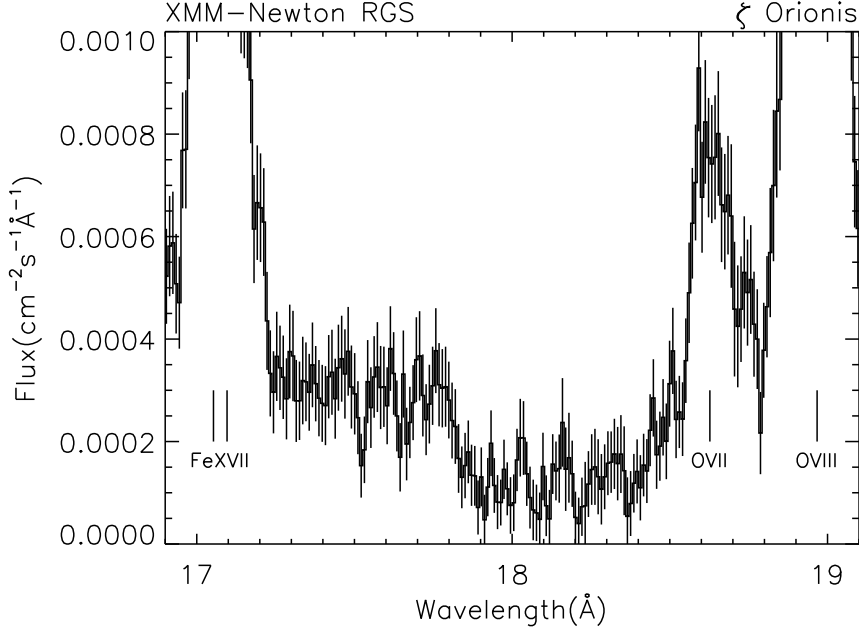


**Fig. 8.** The *XMM-Newton* RGS spectrum of  $\zeta$  Orionis between the lines of Fe XVII  $\lambda\lambda$ 17.053, 17.098 and O VII  $\lambda$ 18.627 and O VIII  $\lambda\lambda$ 18.967, 18.972. Some of the weak lines between about 17.8 and 18.4 Å are probably transitions to the excited  $2s2p^6$  level of Fe XVIII, which appear in the ATOMDB and CHIANTI line lists with uncertain wavelengths. The level of the continuum looks to be less than about  $5 \times 10^{-5} \text{cm}^{-2} \text{s}^{-1} \text{Å}^{-1}$  in this part of the spectrum.



## 5. Origin of the X-rays from $\zeta$ Orionis

The measured fluxes and velocity widths of the lines in the X-ray spectrum of  $\zeta$  Orionis are plotted in Fig. 9. The fluxes have been converted to emission measures using the ATOMDB<sup>2</sup> maximum emissivities, similar to the plots against temperature for  $\zeta$  Puppis by Kahn et al. (2001) and  $\delta$  Orionis by Miller et al. (2002). In common with those and other stars, the X-ray emission measures are three or four orders of magnitude below that available in the wind as a whole and show that only a small fraction of the wind material is involved.

The remarkable thing about Fig. 9 is the lack of any substantial variation with wavelength of either emission measure or velocity width, in contrast to the rough expectations of the instability-driven shock model also plotted there. These have been calculated for the parameters of  $\zeta$  Orionis in Table 1 assuming a velocity law  $v(r) = v_\infty(1 - R_*/r)^\beta$  with  $\beta = 0.8$ . In the development of standard model following Waldron & Cassinelli (2001)'s first discussion of  $\zeta$  Orionis's *Chandra* grating spectrum, X-rays at shorter wavelengths are thought to emerge from deeper into the slower, denser material of the acceleration zone of the wind as the opacity decreases, with the corresponding expected increase in the emission measure plotted in Fig. 1. Yet the measurements show little or no evidence of this. Rather they give quantitative expression to the impression of Fig. 1 that the spectrum is more-or-less optically thin. If this is the case, then the suggestion is that X-rays are not from the dense central regions of the acceleration zone but from further out in the terminal velocity region, although a more precise location is not known. How this might be reconciled with the apparently firm conclusions concerning the location of the X-ray emission deduced from analysis of the He-like triplets is one of the topics discussed below.

In the following sections, an attempt is made to discuss in some detail the feasibility and consequences of the possibility that X-rays arise in the wind's terminal velocity regime. It should be stressed that, in common with any ideas, success or failure should be judged by three things: consistency with the law of physics; ability to reproduce current data, such as those in Fig. 9; and ability to allow predictions to be made that can be tested against future observations.

To begin with, it is tempting to interpret the simultaneous presence in the spectrum of lines of a range of ionization potentials as proof of the presence of a range of temperatures, lending support to the proposal that cooling rather than isothermal shocks are responsible for the X-ray emission. For  $\zeta$  Orionis, using the well-known methods offered, for example, by XSPEC or SPEX<sup>3</sup>, it is possible to make a good synthesis of the spectrum with a multi-temperature model involving gas in collisional ionization equilibrium between about 1MK and 7MK involving either a limited number of discrete temperature components or a continuous DEM distribution, like that suggested by Fig. 9. However, before accepting at face value the temperatures that this would imply, it is worth considering the general physical principles discussed by Zel'dovich & Raizer (2002) that govern shocks and how these might affect their development in the particular circumstances

<sup>2</sup> <http://xc.harvard.edu/atomdb/>

<sup>3</sup> <http://www.sron.nl/divisions/hea/spex/>

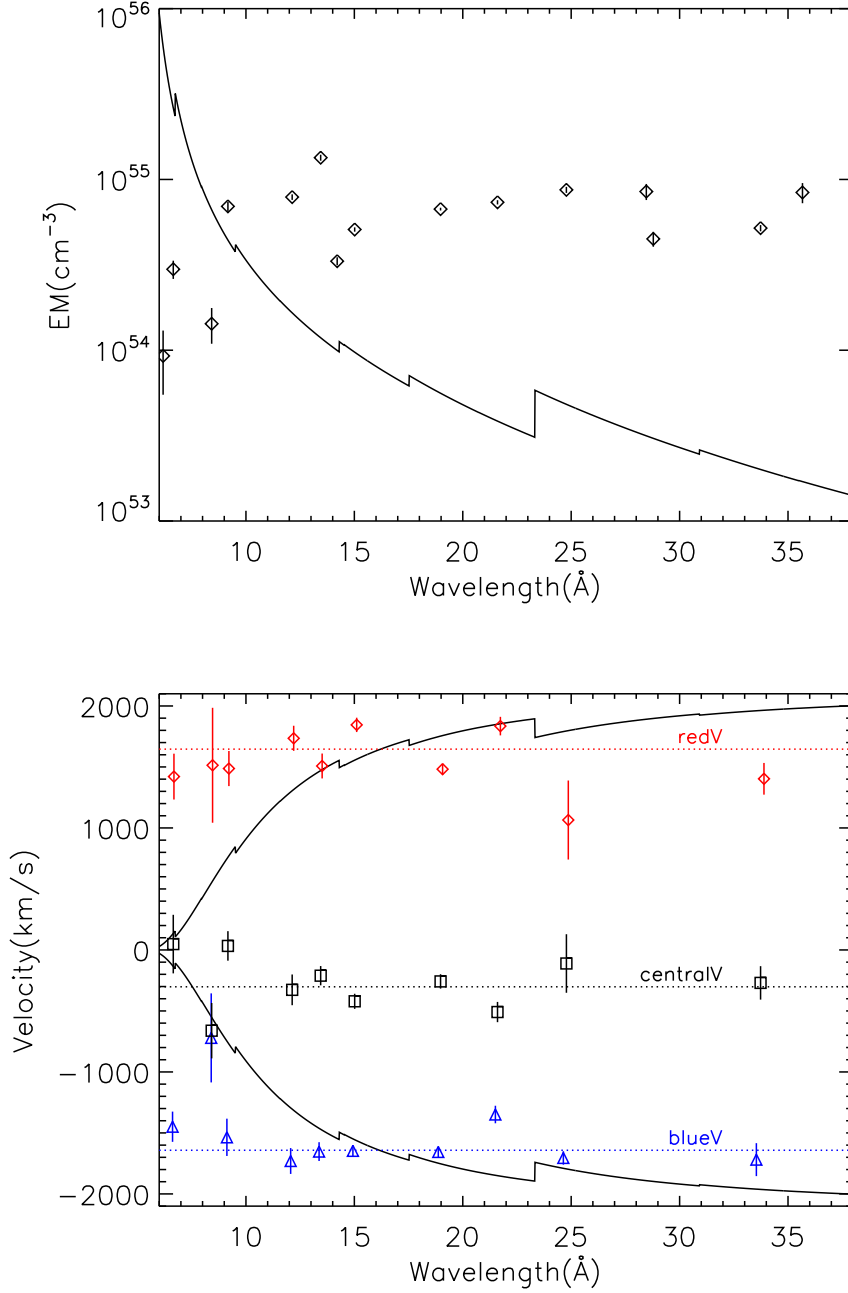


**Fig. 9.** Observed properties of the X-ray lines of  $\zeta$  Orionis. In the top panel are plotted the line emission measures,  $EM = 4\pi d^2(f/\epsilon_{\max})$ , calculated from the measured fluxes,  $f$ , of Table 7, the maximum solar-abundance APED emissivities,  $\epsilon_{\max}$ , and the distance,  $d$ , to the star. The small error bars reflect the high precision with which the fluxes are known. Below are plotted the measured redV, centralV and blueV parameters of the TriLine models of individual line profiles from Table 6, with the corresponding mean values shown by the horizontal lines. Also shown as solid lines are two illustrative quantities calculated for  $R_{\tau=1}(\lambda)$ , the radius of the  $\tau = 1$  X-ray absorption optical depth for a  $\beta = 0.8$  velocity law. At the top is  $EM(> R_{\tau=1}(\lambda))$ , the emission measure outside  $R_{\tau=1}(\lambda)$ , scaled down to overlap the data. Below is  $\pm v(R_{\tau=1}(\lambda))$ , the range of velocities offered by the accelerating wind at that radius.

of a stellar wind, especially if the shocks occur in the relatively low density terminal velocity region. Recently Pollock et al. (2005) did this type of analysis for the binary-system colliding-wind shocks in WR 140. Similar considerations for single hot stars lead to some interesting conclusions.

### 5.1. The nature of shocks in O-star winds

An O-star wind is a plasma flow in which particle interactions are long-range Coulomb collisions. These have a key role in the wind acceleration mechanism in normal circumstances as Coulomb coupling is responsible for redistribution of momentum from the small minority of UV-driven ions to the rest of the flow (e.g. Kudritzki & Puls, 2000). In more extreme conditions, Zel'dovich & Raizer (2002) described the particular properties of plasma shock waves that result from the slow character of the Coulomb energy exchange among ions and even slower between ions and electrons. Because most of the kinetic energy of the flow is in the ions, the most important quantity that determines shock development is the ion-ion collisional mean-free path, which can be estimated as the distance required to deflect by  $90^\circ$  through successive Coulomb collisions a proton or He nucleus moving with the velocity,  $v = v_8 \times 1000 \text{ km s}^{-1}$ . Following Draine & McKee (1993) after Spitzer (1962), the mean-free-path is

$$l_{i-i} \sim 7.0 \times 10^{18} v_8^4 / n_i \text{ cm} \quad (1)$$

where  $n_i$  is the ion density. Fig. 10 shows how the ion-ion collisional mean-free path varies throughout the wind of  $\zeta$  Orionis.

Close to the photosphere, where the density is high and the velocity low,  $l_{i-i}$  is small, but then increases rapidly with the increasing velocity and falling density. At about  $3R_*$  above the stellar surface in the acceleration zone,  $l_{i-i} \approx 0.1R_*$  while at  $10R_*$ ,  $l_{i-i} \approx R_*$ . The implications are profound. If strong shock discontinuities are to develop at all in an O-star wind then some other dissipation mechanism than collisions must come into operation: they must be collisionless shocks. As discussed by Draine & McKee (1993), for example, collisionless shocks probably account for the majority of shocks observed in cosmic plasmas, which are of predominantly low density and thus of long collisional mean-free-path. Familiar examples are the interaction between the solar wind and the earth's magnetosphere and the blast wave of a SNR sweeping through the interstellar medium; more relevant might be the colliding-wind shocks of WR 140 (Pollock et al., 2005). In all these cases, shock dissipation occurs through collective plasma processes involving a magnetic field in which a small characteristic dissipation length is set by the ion Larmor radius. The development of shocks in single stars and the production of X-rays is thus likely to be a phenomenon controlled by magnetic fields at large within the wind.

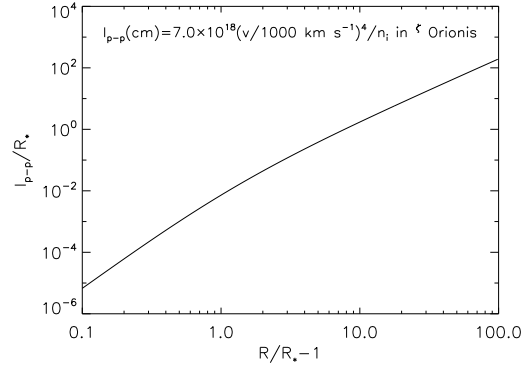


**Fig. 10.** The mean free path for ion-ion Coulomb collisions in the wind of  $\zeta$  Orionis.

### 5.2. Post-shock relaxation and the electron temperature

As described by Zel'dovich & Raizer (2002), a property of plasma shock transitions is that ions are heated to high temperatures while electrons initially remain relatively cold. This is certain for shocks in media dense enough for Coulomb collisional dissipation to operate but is probably also largely true in collisionless shocks, according to the recent review by Rakowski (2006). Although the amount of electron shock heating by plasma turbulence above the minimum provided by adiabatic heating remains a matter of speculation, Rakowski showed that the evidence from SNR shocks is that electron heating decreases with shock velocity and should be small for the few thousand  $\text{km s}^{-1}$  typical of stellar-wind terminal velocities. It is in the subsequent flow through the post-shock relaxation layer that energy is transferred from ions to electrons as the plasma moves towards equilibrium. Naturally enough, for the use of equilibrium plasma models to be justified in the post-shock gas, equilibrium between ions and electrons needs to have been established.

Assuming post-shock bulk energy redistribution takes place through Coulomb collisions, two stages are expected, first amongst ions and then between ions and electrons. During both these stages, the ionization state will also be moving from that of the pre-shock gas towards its relaxed state. Post-shock equilibrium would apply once all these various stages have run to completion. We suggest that the time-scales are too long for this to happen.

Spitzer (1962), Krall & Trivelpiece (1986, section 6.4) and Zel'dovich & Raizer (2002), for example, showed that equilibration between ions and electrons is much slower than between electrons or ions among themselves because of the large difference in mass between ions and electrons. Spitzer (1962) estimated about a factor of 50 slower than ion-ion equilibration from the square root of the mass ratio for modest departures from equipartition.

Immediately behind a stellar wind shock, conditions are far from equilibrium. Brown et al. (2005) have made rigorous calculations of the rate of temperature equilibration, incorporating simultaneous Coulomb scattering on short scales and collective plasma heating on large scales, for arbitrary ion and electron temperatures,  $T_i$  and  $T_e$ . Energy transfer is governed by the term

$$d(T_i - T_e)/dt \propto \kappa_i^2 \kappa_e^2 \frac{(\beta_i m_i \beta_e m_e)^{1/2}}{(\beta_i m_i + \beta_e m_e)^{3/2}} \quad (2)$$

where  $\kappa_i^2 = \beta_i e_i^2 n_i$  and  $\beta_i = 1/T_i$ . This equation shows that in the very earliest stages of relaxation, when ion and electron random velocities are similar and  $T_i \gg T_e$ , the electrons will initially heat up quickly in a time proportional to  $(m_i m_e)$  intermediate between those of electrons and ions among themselves. As the electrons heat up, the fraction of energy  $(m_e/m_i)$  transferred in a collision has less effect and the rate slows down to the factor  $\sqrt{m_e/m_i}$  times ion-ion rate calculated by Spitzer.

Thus, the length scale for post-shock electron heating in the wind of an O star compared to the ion-ion mean-free-path of Fig 10 is likely to be many stellar radii in which case the hot gas may not be able to survive long enough for equilibrium to be established. The low X-ray emission measures of O-stars show that only a small fraction of the wind material is involved, the vast

bulk of which is cold: shocked gas will soon get mixed back with cool material and disappear from view. In this time, there will be little chance for electrons to be heated enough to be able to contribute to the observed X-ray emission by either ionization or bremsstrahlung continuum. A scarcity of shock-heated electrons in the winds of O stars would give rise to a weak continuum and require an alternative means of producing the high levels of ionization.

### 5.3. X-ray ionization by ion-ion interactions in O-star winds

In the supposed absence of shock-heated electrons, what is the origin of the ion species unambiguously identified in the X-ray spectrum? Ions in general and protons in particular in the immediate post-shock gas are probably responsible, as anticipated in general terms by Mewe (1999, p. 148). Through the initial shock transition, the ionization balance is not changed although ions characteristic of the partially ionized cool wind suddenly find themselves in a hostile environment: encounters take place with other ions at relative velocities caused by randomization of the bulk velocity of the pre-shock gas of about  $2000 \text{ km s}^{-1}$  in the terminal velocity regime of  $\zeta$  Orionis. Protons of such velocities are a similarly effective agent for ionization and excitation as electrons of a few keV because the cross-sections depend on the relative velocity of the incident ionizing particle and the velocity of the bound electron, whose order of magnitude is fixed by the Bohr velocity  $v_{\text{Bohr}} = 2188 \text{ km s}^{-1}$ . We suggest that it is the coincidence of this microscopic atomic value of  $v_{\text{Bohr}}$  - widely used as the atomic unit of velocity - and the macroscopic terminal velocities of  $\zeta$  Orionis and other O stars, that is the basic physical reason for the production of X-rays in hot stars.

The relaxing material contains no neutral atoms but is still far from the fully-ionized state discussed by Spitzer and others, so that the same ion-ion interactions involved in energy exchange via Coulomb collisions are likely simultaneously to affect the remaining bound electrons, with possible observational consequences. The ion-ion Coulomb cross-section of  $1/n_i l_{i-i} \sim 7 \times 10^{-21} \text{ cm}^2$  estimated from equation (1), which determines the rate of energy exchange in elastic collisions between ions in the post-shock gas, serves as a benchmark in the discussion below against which the effectiveness may be judged of inelastic processes that also occur during relaxation. High-velocity encounters between ions have maximum inelastic cross-sections of order  $10^{-16} \text{ cm}^2$  that exceed the Coulomb cross-section by orders-of-magnitude and thus might be expected to dominate post-shock relaxation as discussed in more quantitative terms below.

Ion-ion interactions that involve bound electrons are of three types, namely ionization, excitation and charge exchange. Ionization and charge exchange are both mechanisms of electron loss that lead to changes in the ionization state and so could be responsible for the highly-charged ions observed in the X-ray spectrum. Excitation and sometimes charge exchange leave ions in excited states from which decay leads to observable radiation including X-rays. A typical recombination cross-section is of order  $10^{-21} \text{ cm}^2$  and too small to compete with radiative de-excitation in X-ray production.

### 5.3.1. Ion-ion ionization

Ion-atom ionization has been discussed in detail by Kaganovich et al. (2006), whose scaling law for the ionization cross-section by a fully-stripped projectile ion of charge  $Z_p$  and velocity  $v$  of one of the  $N_{nl}$  electrons bound in a quantum state  $(n, l)$  of ionization potential  $I_{nl}$  to a target nucleus of charge  $Z_T$  is given by

$$\sigma^{ion}(v, I_{nl}, Z_p) = \pi a_0^2 \frac{Z_p^2}{(Z_p/Z_T + 1)} N_{nl} \frac{E_0^2}{I_{nl}^2} G\left(\frac{v}{v_{nl} \sqrt{Z_p/Z_T + 1}}\right) \quad (3)$$

where atomic units for cross-section, velocity and energy are defined by the Bohr cross-section  $\pi a_0^2 = 0.880 \times 10^{-16} \text{ cm}^2$ ;  $v_0 = v_{\text{Bohr}} = 2188 \text{ km/s}$ ; and  $E_0 = m_e v_0^2 = 27.2 \text{ eV}$ , respectively. This equation shows in particular how ion-ion ionization cross-sections depend sensitively through the scaling function  $G(v/v_{\text{max}})$  on the relative velocity of the incident ionizing particle and the bound electron. The maximum cross-section,  $\sigma_{\text{max}}$ , is given by  $G(1) \sim 0.8$  at  $v = v_{\text{max}} = v_{nl} \sqrt{Z_p/Z_T + 1}$ .

The velocity of a bound electron is roughly  $v_{nl}/v_0 \sim Z_T/n \sim \sqrt{2I_{nl}/E_0}$ . In the immediate post-shock gas of a stellar wind, the relative velocity scale of ion-ion encounters is fixed by the randomized terminal velocity  $v_\infty$ , though the Maxwellian distributions will ensure that a fraction of encounters also take place at relative velocities up to a few times this value. Kaganovich et al. (2006) showed that their scaling law

$$G(x) = \frac{\exp(-1/x^2)}{x^2} [1.26 + 0.283 \ln(2x^2 + 25)], \quad (4)$$

which falls away from the maximum towards the lower velocities of interest here, reproduces well a variety of observational data for  $x > 0.5$ , at which point the ionization cross-section has fallen to 20% of its maximum value. At low velocities, measurements become difficult because, to quote Kaganovich et al., the ionization cross-section is completely dominated by charge exchange, whose cross-section is comparable to  $\sigma_{\text{max}}$ .

### 5.3.2. Ion-ion charge exchange

Charge exchange between ions is likely to be of fundamental importance in the immediate post-shock gas in the wind of a hot star and be responsible for production of many highly-charged ions. Following Bransden & McDowell (1992, pp. 11-15), a simple theoretical estimate for the low-velocity charge exchange cross-section between a bare nucleus projectile of charge  $Z_p$  interacting with a target nucleus of charge  $Z_T$  with a single bound electron of principal quantum number  $n$  may be written

$$\sigma^{CE}(Z_p, Z_T) = \pi a_0^2 \left( \frac{2n^2(Z_T + 2\sqrt{Z_p Z_T})}{Z_T^2} \right)^2 \quad (5)$$

independent of velocity for  $v/v_{nl} < (Z_p/4Z_T)^{1/4}$ . This expression reproduces experimental data well for electron capture by ions from atomic hydrogen and if applied to collisions between protons ( $Z_p = 1$ ) and, say,  $\text{O}^{7+}$  ( $Z_T = 8$ ) ions, predicts a cross-section of  $1.6 \times 10^{-17} \text{ cm}^2$ . Crossed-beam measurements of collisions between other ions have been reported, for example,



by Skiera et al. (2001), von Diemar et al. (2001) and Bräuning et al. (2005) and show similar or higher cross-sections. including more than  $10^{-16}\text{cm}^{-2}$  for the production of  $\text{N}^{5+}$  from charge exchange with  $\alpha$ -particles: this is interesting because N VI lines appear in the X-ray spectrum of  $\zeta$  Orionis.

### 5.3.3. Implications for post-shock relaxation and the X-ray spectrum

These high cross-sections, which overwhelm Coulomb collisions, guarantee that the first thing to happen to ions in the post-shock relaxation layer concerns their outer bound electrons with charge exchange and ionization leading to rapid readjustment of the ionization balance. This even takes place faster than relaxation among different ions to a common temperature. This conclusion is probably of more general significance. In SNRs, as calculated by Hughes & Helfand (1985) for example, it has often been assumed that the post-shock ionization balance changes in response to hot electrons, whereas particularly for the shocks velocities of a several thousand  $\text{km s}^{-1}$  of some of the remnants discussed by Rakowski (2006), ion-ion interactions are also important, as in the charge-exchange layer immediately behind some SNR shocks discussed by Draine & McKee (1993, p. 403), for example.

For O-star winds, we propose that it is also ion-ion interactions and notably charge exchange during the initial phase of post-shock relaxation that give the observed X-rays. While there seems little doubt that the necessary ions can be produced, the generation of the X-ray spectrum is more uncertain. This may be due to excitation by ions, mainly protons; charge exchange into excited states in the hot gas; or charge exchange in eventual encounters with the much less tightly bound electrons in the plentiful supply of much cooler ions in nearby unshocked material that makes up the great majority of the wind. This final possibility seems worthy of future work. If proton ionization is significant, while it is not expected that the great majority of free electrons will be heated much immediately behind the shock, a small population of hot secondary electrons would be ejected, giving some scope for a bremsstrahlung continuum.

### 5.4. *The velocity profile of the X-ray lines*

Most of the efforts made so far to account for the shape of the X-ray lines in hot stars, such as those of Ignace & Gayley (2002), Kramer et al. (2003) and Oskinova et al. (2004), have assumed that the X-ray emitting gas is moving with the majority cool gas. By doing so and appealing to the velocity law of the cool gas, attempts have been made to constrain the location of the hot gas. In particular, it has regularly been argued that the red wing of the X-ray lines arises in material in the wind on the far side of the star flowing away from the observer. This simple assumption is hard to justify, if only because much of the ordered motion of the wind needs to be converted to heat for X-rays to be observed at all and, for CIE models, half the energy has to be transferred from ions to electrons for excitation to occur.

For an ideal gas of mean particle mass  $m$  flowing at velocity  $v$  into a strong stationary shock, the jump conditions determine the equilibrium temperature and velocity of the outflowing shocked gas to be  $kT_S/m = (3/16)v^2$  and  $v_S = v/4$ . For material of solar composition,  $kT_S \sim 1.2v_8^2$  keV, where  $v = v_8 \times 1000 \text{ km s}^{-1}$ , so that the observation of X-ray gas in equilibrium near the 0.5 keV of Table 3 would imply the complete dissipation of about  $650 \text{ km s}^{-1}$  of directed kinetic energy.

Out of equilibrium, it is more likely that the observed line velocity profiles mostly reflect instead the line-of-sight component of the thermalized motion of ions in the immediate post-shock gas. For a Maxwellian distribution,

$$\text{HWHM}(v_x) = \sqrt{2 \ln 2 (kT_S/m)} = (\sqrt{6 \ln 2/4})v \sim 0.51v. \quad (6)$$

The similar observed widths of different ions further implies that even equilibration between ions does not take place.

In addition to this thermal component, the bulk flow away from the shock at  $v_S = v/4$  will also contribute to the line profile. The calculations that Ignace & Gayley (2002) made for material moving at constant radial velocity in the terminal velocity flow, may equally well be applied to this slower-moving material. The resultant, roughly triangular, line profiles show blue-shifted peaks at 10 or 20% of the outflow velocity, depending on the optical depth, and a half width of about 60%. The resultant combination of thermal and bulk motions should then shift the line to the blue by a fraction of the terminal velocity with a width mostly determined by the greater random motion.

The observed lines in  $\zeta$  Orionis are roughly consistent with this scheme, showing blue-shifted peaks of about  $v_\infty/7$  and half-widths of about 80% of the value of  $0.51v_\infty$  expected for complete thermalization of gas moving at the terminal velocity. While it is conceivable that the X-ray emission is picking out the small amount of gas in the wind-acceleration zone travelling at this fraction of the terminal velocity, we consider this unlikely, not least because of the apparent lack of X-ray absorption.. Two further possibilities come to mind: either that the shocks are not stationary in the wind but are moving outwards at a few hundred  $\text{km s}^{-1}$  and are completely thermalized; or that the shocks are stationary and occur throughout the terminal velocity regime and the energy balance involves other channels than merely the production of heat. As non-thermal particle acceleration is a common feature of collisionless shocks, such as those in SNRs and those probably in WR 140, we consider this possibility the more promising, although free-free emission and absorption by the cool wind is expected to be strong enough to prevent any non-thermal radio radiation from being observed.

### 5.5. Absence of equilibrium in the post-shock plasma and the He-like triplets

If O-star X-rays are produced by terminal-velocity shocks in the wind, then the sluggishness of energy exchange throughout the post-shock gas will prevent the establishment of equilibrium before the hot gas is overwhelmed by cool material. Therefore, the use of coronal equilibrium

models to analyse O-star X-ray spectra is unlikely to yield any physically meaningful information about conditions in the hot gas, though it is always possible to derive equivalent equilibrium temperatures like those quoted above for  $\zeta$  Orionis and elsewhere for other stars. The X-ray spectrum is more likely to reflect the individual cross-sections of the three important processes between ions discussed above of charge exchange, ionization and excitation.

An argument in support of the instability-driven shock model has been its success following Kahn et al. (2001) and Waldron & Cassinelli (2001) in accounting for the characteristic patterns of the *fir* lines of the He-like triplets: in contrast to most other high-resolution X-ray spectra, the O-star intercombination lines are particularly strong, showing the effects of photospheric UV pumping of the  $^3S_1$  upper level of the forbidden line to  $^3P_{1,2}$  upper levels of the intercombination line. In  $\zeta$  Puppis, Kahn et al. (2001) showed that there is enough radiation that the photoexcitation rate exceeds the intercombination line decay rate with a radius that varies from about  $3R_*$  for Si XIII to  $200R_*$  for N VI, so that the UV affects an enormous volume of the wind.

Calculations of the expected line ratios such a UV field, such as those of Porquet et al. (2001), have been based on otherwise equilibrium conditions. In the rarefied gas immediately behind the collisionless shock in an O-star wind imagined above, apart from the intense UV radiation environment, other conditions are expected to be quite different with the He-like ratios subject to a variety of considerations, namely:

- a plasma out of equilibrium
- a scarcity of hot electrons
- energy concentrated in interacting ions
- widespread charge exchange
- ionization by non-thermal particles

Hot protons and cool electrons are expected to have similar random velocity distributions and thus both contribute to collisional coupling of the He-like triplet levels. Proton excitation leads to different line ratios because of the absence of resonances and exchange terms (e.g. Shevelko & Vainshtein, 1993, p. 41).

Charge exchange is likely to be as important in stellar winds as it is for the generation of cometary X-rays by charge exchange of neutral material with highly-charged ions in the solar wind. In laboratory measurements designed to simulate cometary charge exchange by Beiersdorfer et al. (2003), which are at very low velocities on the atomic scale, the forbidden line was strongly enhanced. In the crossed-beam measurements discussed above at higher relative velocities more relevant to hot stars, though still low on the atomic scale, the total cross-sections are dominated by charge exchange.

Although, following the suggestion by Pollock (1987), most authors have cited inverse-Compton emission as a non-thermal signature, ionization losses are a more important cooling mechanism of mildly relativistic particles. This may be an opportunity to observe, at least indirectly, the effects of cosmic-ray acceleration in single stellar winds through the detection of

satellite lines following inner-shell ionization (e.g. Mewe & Schrijver, 1978), which may also cause the unusually strong He-like forbidden lines in the colliding-wind spectra  $\eta$  Carinae and WR 140 (Pollock et al., 2005). Incidentally, there may be some evidence of satellite lines in the O VII triplet of  $\zeta$  Orionis in which the intercombination line appears significantly blue-shifted from the wavelength expected from the ensemble of other lines by  $-13 \pm 3$  mÅ. This partly accounts for the extra blue shift of O VII in Table 6.

In summary, some theoretical effort will be required to calculate the X-ray spectrum in general and the He-like line ratios in particular to be expected from shocked ions in an O-star wind before proper conclusions can be drawn about the effects of UV radiation and the implications for the location of the X-ray emitting material.

## 6. X-ray absorption in O-star winds

In spite of the high optical depths expected on the basis of supposedly well-determined mass-loss rates, Kahn et al. (2001) showed the lack of any detectable absorption edges in  $\zeta$  Puppis. Even cursory inspection of  $\zeta$  Orionis's RGS spectrum or those of other O-stars (e.g. Paerels & Kahn, 2003) shows no obvious sign of absorption, as emphasized by the strength of C VI Ly $\alpha$ .

An important part of attempts to reconcile the observational data with an origin deep in the wind's acceleration zone within a few stellar radii of the surface has involved seeking means of reducing the X-ray opacity. From a theoretical point-of-view, Waldron & Cassinelli (2001) and Cassinelli et al. (2001) used the reduced opacities of Waldron et al. (1998) from self-consistent calculations of the ionization balance to be expected in the presence of UV and X-radiation (MacFarlane et al., 1993, 1994). Independently, Kramer et al. (2003), for example, appealed to significantly reduced attenuation in their models of the  $\zeta$  Puppis X-ray line profiles.

It might have been expected that the high UV outer-shell optical depths necessary for the line driving would guarantee a correspondingly high X-ray inner-shell optical depth. It has been known for many years that this is indeed the case, as demonstrated by the bright neutron star hard X-ray sources powered by accretion from an otherwise normal hot star. Vela X-1 (e.g. Sako et al. (1999) and references cited there) is a relevant example as the primary star HD 77581 is a B0.5Iab star of similar spectral type to  $\zeta$  Orionis. The neutron star orbits at about  $0.78R_*$  above the surface of the supergiant, in what would otherwise be the strongest region of the acceleration zone. It is a simple observational fact that the neutron-star secondary's X-rays are subject to heavy absorption. While this varies through the orbit, reaching values of several times  $10^{23}\text{cm}^{-2}$ , much of it is due to the rearrangement of wind material into an accretion wake that trails the neutron star. The X-ray absorption, though occasionally extremely high, is well modelled by cold material.

Immediately after eclipse, on the other hand, when the line-of-sight passes only through the stellar wind, a minimum column density of about  $2 \times 10^{22}\text{cm}^{-2}$  is observed.. This value is reasonably close to that expected if  $\zeta$  Orionis were to take the place of HD 77581. For a

spherically symmetric wind with a  $\beta$  velocity law, the integrated column density between a point distance  $R$  from the surface of the star along the line-of-sight scales as

$$N_R(R, \phi, i) \sim (\dot{M}/\mu m_p v_\infty R_*) (\gamma / \sin \gamma) H(R, R_*, \beta) \text{ cm}^{-2} \quad (7)$$

where  $\mu$  is the mean atomic number,  $m_p$  the proton mass and  $v(r) = v_\infty(1 - R_*/r)^\beta$ . The column density is the product of a column density characteristic of the star,  $N_* = (\dot{M}/\mu m_p v_\infty R_*)$ , and two scaling factors: a geometrical factor  $(\gamma / \sin \gamma)$ , where  $\cos \gamma = \cos \phi \sin \theta$  and  $\phi, \theta$  are the azimuth and inclination angles between the radial direction through  $R$  and the line-of-sight; and an analytical density-related factor  $H(R, R_*, \beta)$ , which exceeds unity for points in the densest parts of the wind and equals  $(R_*/R)$  far from the stellar surface. For the parameters of  $\zeta$  Orionis in Table 1,  $N_* \sim 7.3 \times 10^{21} \text{ cm}^{-2}$ . For the line-of-sight that would apply to a neutron star emerging from an eclipse by  $\zeta$  Orionis,  $\gamma \sim \pi/2$  leading to  $N_R \sim 1.1 \times 10^{22} \text{ cm}^{-2}$ , only about a factor of two lower the observed value in Vela X-1. The evidence, therefore, is that X-rays produced at  $R = 1.78 R_*$  in the wind of a supergiant companion of similar type to  $\zeta$  Orionis are absorbed. This would equally be expected to apply to any intrinsic X-rays produced here and lead to the rapidly increasing emission measures and decreasing velocities plotted in Fig. 9.

## 7. A new paradigm for the X-ray emission from O stars

We propose that the high inertia of the plasma flow in O-star winds, caused by the weakness of Coulomb interactions, has important consequences for the production of X-rays in the flow. If shocks develop at all, they are collisionless shocks in which the fundamental role of plasma instabilities suggests that the local magnetic field could be the “missing variable” responsible for the scatter of an order-of-magnitude or more in the modest X-ray luminosities generated by otherwise apparently similar O stars.

The long Coulomb collisional mean-free-path, apart from requiring a collisionless shock transition and slow post-shock energy exchange, also more generally limits the steepness of pressure gradients that can be sustained by the medium and defines a minimum size for any structures in the hot gas. In this case, it is unlikely that the microscopic instability in the line-driving mechanism will be able to steepen into the macroscopic shocks widely thought to generate O-star X-rays: the instability would soon be limited by the difficulty of transferring momentum quickly enough from the unstable driven ions to the rest of the wind, causing breakdown of the single-fluid approximation as discussed, for example, for thin hot-star winds by Springmann & Pauldrach (1992). Furthermore, the narrowness of the X-ray line profiles would appear to exclude the type of positive-going velocity instabilities in the calculations of Owocki et al. (1988), for example.

The observed common line profile implies a common seat of X-ray emission for all the ions, a notion qualitatively consistent with an origin in the terminal velocity regime. While X-rays are probably produced throughout the wind as a routine aspect of the chaotic, supersonic flow of magnetized plasma, the observable volume is likely to be limited to some extent by photoelectric

absorption, giving rise to small systematic changes in the line profiles from ion to ion. The line width is mainly due to randomization of the directed kinetic energy of the flow.

A thorough quantitative assessment of these ideas will have to await a detailed emission model that is expected to include, among other things, ionization, excitation and charge exchange averaged over the microscopic velocity distribution of ions in the post-shock gas as well as an energy budget with a non-thermal component.

An inevitable consequence of the scheme proposed is the effective absence of hot electrons in an O-star wind, altering the physical basis of the plasma emission models concerned. In contrast to either ionization by electron impact or photoionization, which together account for the majority of observed X-ray plasmas, single O-star spectra may be one of the clearest examples of a protoionized plasma. The term “protoionized” seems appropriate both for the contrast with photoionized and because it describes the very earliest stages of post-shock relaxation through which tenuous plasmas are bound to pass before electrons become hot enough to take over. The shock transitions themselves, though probably smaller in physical extent than the extensive shocks which span a large-scale colliding-wind flow such as WR 140, initially obey similar jump conditions. The distinction between spectra lies rather in the post-shock layer, in the amount of equilibration that takes place between ions and electrons. If the hot plasma is confined by magnetic fields, as in WR 140, for example, post-shock relaxation may take its long-term course allowing energy to be transferred from ions to electrons, which may then excite a familiar plasma spectrum characteristic of collisional ionization equilibrium. Otherwise, in the winds of single O-stars, the plasma is not in equilibrium, few or no electrons reach high temperatures and we observe instead the effects of the coincidence between the macroscopic terminal velocity of the wind and the microscopic Bohr velocity characteristic of electrons in bound atomic states. Interactions with the majority cool material may also be important.

There are two simple tests of the new scheme which the data available thus far are not quite able to support: long, high-resolution, exposures of single O-stars should be able to establish two characteristics of the X-ray spectrum: first, that all the lines have much the same shape; and second that the continuum is weaker than that from an electron-excited plasma.

*Acknowledgements.* Many thanks are due to Ton Raassen of SRON Utrecht in the Netherlands, who cast a critical eye over many stages of the development of the ideas discussed here.

## References

- Berghöfer, T.W. & Schmitt, J.H.M.M. 1994, *A&A*, 290, 435
- Berghöfer, T.W., Schmitt, J.H.M.M., & Cassinelli, J.P. 1996, *A&AS*, 118, 481
- Beiersdorfer, P., Boyce, K.R., Brown, G.V., et al. 2003, *Science*, 300, 1558
- Bransden, B.H. & McDowell, M.R.C. 1992, *Charge Exchange and the Theory of Ion-Atom Collisions*, Oxford: Clarendon Press
- Bräuning, H., Trassi, R., Theiß, A., et al. 2005, *J. Phys. B*, 38, 2311

- Brown, L.S., Preston, D.L., & Singleton, R.L.Jr 2005, *Physics Reports*, 410, 237
- Cassinelli, J.P., Miller, N.A., Waldron, W.L., MacFarlane, J.J., & Cohen, D.H. 2001, *ApJ*, 554, L55
- den Herder, J.W., Brinkman, A.C., Kahn, S.M., et al. 2001, *A&A*, 365, L7
- de Zeeuw, P.T., Hoogerwerf, R., de Bruijne, J.H.J., Brown, A.G.A., & Blaauw, A. 1999, *AJ*, 117, 354
- Diplas, A. & Savage, B.D. 1994, *ApJS*, 93, 211
- Draine, B.T. & McKee, C.F. 1993, *ARA&A*, 31, 373
- Feldmeier, A., Kudritzki, R.-P., Palsa, R., Pauldrach, A.W.A., & Puls, J. 1997, *A&A*, 320, 899
- Hughes, J.P. & Helfand, D.J.. 1985, *ApJ*, 291, 544
- Hummel, C.A., White, N.M., Elias II, N.M., Hajian, A.R., & Nordgren, T.E. 2000, *ApJ*, 540, L91
- Ignace, R. & Gayley, K.G. 2002, *ApJ*, 568, 954
- Jansen, F., Lumb, D., Altieri, B., et al. 2001, *A&A*, 365, L1
- Kaganovich, I.D., Startsev, E. & Davidson, R.C. 2006, *New Journal of Physics*, in press
- Kahn, S.M., Leutenegger, M.A., Cottam, J., et al. 2001, *A&A*, 365, L312
- Krall, N.A. & Trivelpiece, A.W. 1986, *Principles of Plasma Physics*, San Francisco Press
- Kramer, R.H., Cohen, D.H., & Owocki, S.P. 2003, *ApJ*, 592, 532
- Kudritzki, R.-P. & Puls, J. 2000, *ARA&A*, 38, 613
- Lamers, H.J.G.L.M., Haser, S., de Koter, A., & Leitherer, C. 1999, *ApJ*, 516, 872
- MacFarlane, J.J., Waldron, W.L., Corcoran, M.F., et al. 1993 *ApJ*, 419, 813
- MacFarlane, J.J., Cohen, D.H., & Wang, P. 1994, *ApJ*, 437, 351
- Mason, K.O., Breeveld, A., Much, R., et al. 2001, *A&A*, 365, L36
- Mewe, R. 1999, *Lecture Notes in Physics* (Springer Verlag, Berlin), 520, 109.
- Mewe, R. & Schrijver, J. 1978, *A&A*, 65, 99
- Miller, N.A., 2002, PhD thesis, University of Wisconsin.
- Miller, N.A., Cassinelli, J.P., Waldron, W.L., MacFarlane, J.J., & Cohen D.H. 2002, *ApJ*, 577, 951
- Oskinova, L.M., Feldmeier, A., & Hamann, W.-R. 2004, *A&A*, 422, 675
- Owocki, S.P., Castor, J.I., & Rybicki, G.B. 1988, *ApJ*, 335, 914
- Paerels, F.B.S. & Kahn, S.M. 2003, *ARA&A*, 41, 291
- Pollock, A.M.T. 1987, *A&A*, 171, 135
- Pollock, A.M.T., Corcoran, M.F., Stevens, I.R., & Williams, P.M. 2005, *ApJ*, 629, 482
- Porquet, D., Mewe, R., Dubau, J., Raassen, A.J.J., & Kaastra, J.S. 2001, *A&A*, 376, 1113
- Prinja, R.K., Barlow, M.J., & Howarth, I.D. 1990, *ApJ*, 361, 607
- Raassen, A. J. J., Mewe, R., Audard, M., et al. 2002, *A&A*, 389, 288
- Rakowski, C.E. 2006, *Advances in Space Research*, 35, 1017
- Rybicki, G.B. & Lightman, A.P. 1979, *Radiative Processes in Astrophysics*, New York: Wiley
- Sako, M., Liedahl, D.A., Kahn, S.M., & Paerels, F. 1999, *ApJ*, 525, 921

- Shevelko, V.P. & Vainshtein, L.A. 1993, *Atomic Physics for Hot Plasmas*, Bristol: Institute of Physics
- Skiera, D., Trassi, R., Huber, K., et al. 2001, *Physica Scripta*, T92, 423
- Smith, R.K., Brickhouse, N.S., Liedahl, D.A., & Raymond, J.C. 2001, *ApJ*, 556, L91
- Spitzer, L. Jr. 1962, *Physics of Fully Ionized Gases*, New York: Wiley, 2nd ed.
- Springmann, U.W.E. & Pauldrach, A.W.A. 1992, *A&A*, 262, 515
- Strüder, L., Briel, U., Dennerl, K., et al. 2001, *A&A*, 365, L18
- Turner, M.J.L., Abbey, A., Arnaud, M., et al. 2001, *A&A*, 365, L27
- von Diemar, K., Melchert, F., Huber, K., et al. 2001, *J. Phys. B*, 34, L93
- Waldron, W.L., Corcoran, M.F., Drake, S.A. & Smale, A.P. 1998, *ApJS*, 118, 217
- Waldron, W.L., & Cassinelli, J.P. 2001, *ApJ*, 548, L45
- Young, P.R., Del Zanna, G., Landi, E., Dere, K.P., Mason, H.E., & Landini, M. 2003, *ApJS*, 144, 135
- Zel'dovich, Ya.B. & Raizer, Yu.P. 2002, *Physics of Shock Waves and High-Temperature Hydrodynamic Phenomena* (Mineola, New York: Dover)



**Table 7.** Fluxes of the X-ray lines in  $\zeta$  Orionis using the TriLine model of Table 3 for each line.

Ion	$\lambda_{\text{lab}}$	Line ID	Flux( $10^{-5}\text{cm}^{-2}\text{s}^{-1}$ )
C VI	33.734	Ly $\alpha$	40.90 $\pm$ 1.72
	28.465	Ly $\beta$	6.76 $\pm$ 0.73
	26.990	Ly $\gamma$	1.59 $\pm$ 0.49
S XII	36.398		4.66 $\pm$ 0.97
	36.573		1.31 $\pm$ 0.88
S XIII	35.667		6.96 $\pm$ 0.94
	37.598		3.99 $\pm$ 1.78
	32.242		1.93 $\pm$ 0.68
N VI	28.787	<i>r</i>	7.88 $\pm$ 0.79
	29.084	<i>i</i>	7.48 $\pm$ 0.85
	29.534	<i>f</i>	0.00 $\pm$ 0.25
	24.898	He $\beta$	1.35 $\pm$ 0.73
N VII	24.779	Ly $\alpha$	17.64 $\pm$ 0.72
	20.909	Ly $\beta$	0.26 $\pm$ 0.47
O VII	21.602	<i>r</i>	96.13 $\pm$ 2.73
	21.807	<i>i</i>	75.99 $\pm$ 2.47
	22.101	<i>f</i>	7.69 $\pm$ 0.96
	18.627	He $\beta$	8.41 $\pm$ 0.57
	17.768	He $\gamma$	1.98 $\pm$ 0.36
	17.396	He $\delta$	1.60 $\pm$ 0.36
O VIII	18.967	Ly $\alpha$	92.43 $\pm$ 1.73
	16.005	Ly $\beta$	13.55 $\pm$ 0.75
	15.176	Ly $\gamma$	7.05 $\pm$ 0.75
	14.820	Ly $\delta$	1.12 $\pm$ 0.29
Fe XVII	15.015		37.68 $\pm$ 1.10
	15.262		17.36 $\pm$ 0.83
	15.453		4.45 $\pm$ 0.45
	16.778		19.45 $\pm$ 0.70
	17.053		30.05 $\pm$ 1.65
	17.098		17.03 $\pm$ 1.65
	12.266		1.92 $\pm$ 0.69
Fe XVIII	14.208		7.77 $\pm$ 0.42

Ion	$\lambda_{\text{lab}}$	Line ID	Flux( $10^{-5}\text{cm}^{-2}\text{s}^{-1}$ )
	14.373		4.03±0.36
	14.534		2.79±0.33
	15.625		2.91±0.39
	15.870		1.93±0.35
	16.071		2.96±0.61
	17.623		2.76±0.38
Fe xix	13.518		2.54±1.26
	13.795		3.99±0.38
	15.079		1.23±0.90
Ne ix	13.447	<i>r</i>	20.35±0.82
	13.553	<i>i</i>	11.95±1.07
	13.699	<i>f</i>	3.14±0.39
	11.547	He $\beta$	2.22±0.22
	11.000	He $\gamma$	0.97±0.17
Fe xx	12.824		0.45±0.08
	12.846		0.45±0.08
	12.864		0.45±0.08
Fe xxi	12.284		1.27±0.29
Ne x	12.132	Ly $\alpha$	12.02±0.45
	10.238	Ly $\beta$	1.35±0.16
	9.708	Ly $\gamma$	0.33±0.16
	9.481	Ly $\delta$	0.07±0.15
Mg xi	9.169	<i>r</i>	2.86±0.18
	9.231	<i>i</i>	1.31±0.15
	9.314	<i>f</i>	1.25±0.13
	7.851	He $\beta$	0.26±0.12
Mg xii	8.419	Ly $\alpha$	0.55±0.13
	7.106	Ly $\beta$	0.10±0.09
Si xiii	6.648	<i>r</i>	0.98±0.12
	6.688	<i>i</i>	0.38±0.14
	6.740	<i>f</i>	0.89±0.11
Si xiv	6.180	Ly $\alpha$	0.27±0.11

## List of Objects

‘ $\zeta$  Orionis’ on page 2